Relationships between Hourly Rainfall Intensity and Atmospheric Variables over the Contiguous United States

CHIARA LEPORE

Lamont-Doherty Earth Observatory, Columbia University, Palisades, New York

JOHN T. ALLEN

International Research Institute for Climate and Society, Columbia University, Palisades, New York

MICHAEL K. TIPPETT

Department of Applied Physics and Applied Mathematics, Columbia University, New York, New York, and Center of Excellence for Climate Change Research, Department of Meteorology, King Abdulaziz University, Jeddah, Saudi Arabia

(Manuscript received 8 May 2015, in final form 4 February 2016)

ABSTRACT

Rainfall intensity displays relationships with atmospheric conditions such as surface temperature, and these relationships have implications for how the intensity of rainfall varies with climate. Here, hourly gauge measurements of rainfall over the contiguous United States (CONUS) are related to atmospheric variables taken from the North American Regional Reanalysis for the period 1979–2012. This analysis extends previous work relating the rainfall process to the environment by including a wider range of variables in univariate and bivariate quantile regressions. Known covariate relationships are used to quantify the regional contributions of different weather regimes to rainfall occurrence and to identify preferential atmospheric states for rainfall occurrence. The efficiency of different sets of regressors is evaluated, and the results show that both moisture availability and vertical instability should be taken into account, with CAPE in combination with specific humidity or dewpoint temperature being the most powerful regressors. Different regions and seasons behave differently, pointing to the challenges of constructing global or CONUS-wide models for representing the rainfall process. In particular, the relationships between environment and rainfall in the west of the United States are different from other regions, reflecting nonlocal rainfall processes. Most of the coastal and eastern United States display relatively low regional variability in the relationships between rainfall and environment.

1. Introduction

Rainfall processes occur in response to both synoptic and mesoscale forcing on preexisting conditions within the atmospheric column. However, the relationship between these atmospheric conditions and extreme precipitation is not well understood, especially on a regional basis. Several studies have recently examined the dependence of rainfall on ambient atmospheric variables (Berg et al. 2009; DeGaetano 2009; Groisman et al. 2005; Haerter and Berg 2009; Lenderink and Van Meijgaard 2008; Lenderink and van Meijgaard 2009; Shaw et al. 2011; Utsumi et al. 2011), primarily focusing on the dependence of precipitation intensity on near-surface temperature. These analyses were driven by the question of whether rainfall intensity and extremes will increase at the Clausius–Clapeyron (CC) rate of ~7% K^{-1} as the climate warms.

The CC rate, however, is not expected to represent the regional precipitation response to warming everywhere. In regions with appreciable access to moisture, such as the tropics or continental margins, the total rainfall will likely increase at approximately the CC rate. In certain areas, extreme rainfall intensity, especially for short-duration intense rainfall events, can increase at a higher rate, often referred to as a super-CC rate. One possible explanation for the super-CC rate of extreme rainfall is that a greater release of latent heat in a warmer climate

Corresponding author address: Chiara Lepore, 207 Monell, 61 Rte. 9W, P.O. Box 1000, Palisades, NY 10964-8000.
E-mail: clepore@ldeo.columbia.edu

DOI: 10.1175/JCLI-D-15-0331.1

may produce more intense updrafts (Lenderink and Van Meijgaard 2008). Another interpretation is that the fraction of convective precipitation increases with higher surface temperatures (Haerter and Berg 2009). The influence of a warmer climate on extreme rainfall intensity appears to be more complex over moisture-limited regions or those where advective processes are important (Lepore et al. 2015).

Comparatively little attention has been given in the literature to the dependence of precipitation on nonthermodynamic atmospheric variables or regional characteristics. Several authors have explored the relationships of daily and seasonal rainfall properties with atmospheric states including sea level pressure, geopotential heights, RH, wind components, and CAPE (Molini et al. 2011; Myoung and Nielsen-Gammon 2010; Hertig and Jacobeit 2013), and a few other analyses have looked at both dynamic and thermodynamic predictors of vertical structure in precipitation (Rudolph and Friedrich 2014). In an analysis of eastern U.S. hourly rainfall intensities, Lepore et al. (2015) examined dependencies on both dynamic and thermodynamic predictors, such as temperature, dewpoint temperature, and CAPE, finding that higher quantiles of precipitation ($p > 0.75$) are highly dependent on CAPE. These findings suggest the need to investigate the relationship of rainfall extremes with a wider spectrum of atmospheric variables. Interestingly, Lepore et al. (2015) found that rainfall intensity is better correlated with CAPE from reanalysis than with CAPE computed from atmospheric soundings. This result can be explained by considering the relative proximity of a reanalysis vertical sounding profile compared to observed sounding data. Radiosonde observations are unevenly spaced, typically taken twice daily, and can potentially fail. In contrast, reanalysis data are a model assimilation of available observations and are sampled on a 6- or 3-hourly gridded basis, meaning the environment is often more *proximal*, both in time and space, to the rainfall measurements (Brooks et al. 2003; Allen and Karoly 2014; Gensini et al. 2014). However, during reanalysis, topographically induced processes, as well as synoptic and mesoscale boundaries, can be temporally and spatially displaced, meaning that small-scale features are not as well represented as in a local sounding profile. Despite these limitations, the greater availability of reliable proximity profiles and evaluations compared to soundings has suggested that quantities such as CAPE, convective inhibition (CIN), and wind vectors are representative in reanalysis data, especially within the context of the analysis presented here, and that they can provide useful atmospheric profiles prior to and during rainy hours.

The concept of relating extremes to environmental descriptors, often referred to as an ''ingredients based'' approach, has been extensively used in short-range forecasting. A seminal work by Doswell et al. (1996) applied this methodology to flash flood prediction. Other authors have extended similar approaches to establish the effect of the large-scale environment on the seasonal and annual numbers of tropical cyclones (Camargo et al. 2007; Vecchi et al. 2011; Tippett et al. 2011) and to make projections under climate change scenarios (Camargo et al. 2014). For continental convection, a similar approach has been used to understand the influence of climate variations on severe thunderstorms (Brooks et al. 2003; Trapp et al. 2007; Diffenbaugh et al. 2013), tornadoes (Tippett et al. 2012, 2014), and hail (Allen et al. 2015a). Finally, this approach is also valuable for connecting severe weather events with large-scale climate variations (e.g., Allen et al. 2015b).

The motivation behind this work is to establish relationships between the environment and the rainfall intensity process. A deeper understanding of these links can be used for a variety of scientific applications, for example, to develop new models for the assessment of hydrological hazards. In fact, simple statistical models, such as linear regressions based on these relationships, can provide a way to overcome the spatial limitations of gauge networks and to quantify extreme precipitation risk where there are no gauges.

Here, we link the distribution of hourly rainfall rates with environmental variables (sections 2a and 2b) through the use of univariate and multivariate quantile regressions and conditional distributions (section 3). In particular, we focus on the extremes of the hourly rainfall rate distribution corresponding to percentiles equal or higher than the 75th percentile. The atmospheric variables included in our analysis describe moisture availability (i.e., dewpoint temperature, specific humidity, and RH), vertical instability (i.e., CAPE, CIN, and vertical wind shear), and advective processes (i.e., surface and higher winds). Some of these variables (e.g., CAPE and wind shear) are commonly used in the description of environments favorable to severe weather, and have been used to establish the contribution of convection and severe convection to rainfall extremes (Hitchens et al. 2013). Here, they allow us to gain some understanding of the role of nonconvective, convective, and severe convective processes in the precipitation process as a whole for the entire CONUS (section 4a). We use covariate relationships (section 4a) to discriminate between typically nonconvective, convective, and severe weather environments.

The results (sections 4b–d) compile a wide catalog of rainfall-atmospheric variable dependencies and explore how these dependencies vary regionally and seasonally. This set of results represents a necessary first step

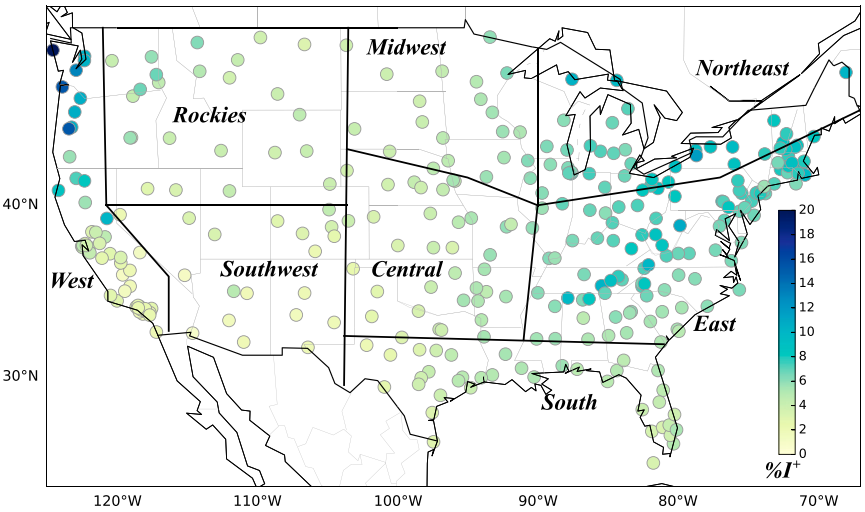

FIG. 1. Locations of the 278 stations (colored circles) with complete records during 1979–2012 and the eight regions. The color coding indicates the annual mean frequency of rainy hours (%).

toward the development of statistical models that link extreme rainfall to atmospheric variables, which is key to the assessment of hydrologic hazards within a nonstationary framework.

2. Data

a. Hourly gauge data

Hourly precipitation intensity values (denoted I) are taken from the NCDC gauge network (available online at http://www.ncdc.noaa.gov/cdo-web/). The data used here cover the period 1979–2012. There are stations in all 50 states, and the number of recording stations varies in time, with recent increases taking the gauge network to almost 5000 sites (Groisman et al. 2012). Eliminating stations with missing or replaced values as in Lepore et al. (2015) results in the 278 stations that are used here and whose locations are shown in Fig. 1. The number of years of complete data available at each station ranges from 1 to 31 with half of the stations having at least 29 years of data. Station data are pooled over the eight regions shown in Fig. 1, to allow more robust estimates of higher quantiles. The region definitions take into account the spatial distribution of available stations and the similarity of rainfall characteristics (Lepore et al. 2015). Data are analyzed on a calendar year and seasonal basis. The four seasons considered are NH winter [December–February (DJF)], spring [March–May (MAM)], summer [June–August (JJA)], and fall [September–November (SON)].

b. North American Regional Reanalysis

Environmental parameters are taken from the North American Regional Reanalysis (NARR Mesinger et al. 2006) over the contiguous United States (CONUS). The NARR data have a native horizontal grid spacing of 32 km, 45 vertical layers, and a temporal resolution of 3 h. Here, the NARR data are first interpolated onto a $1° \times 1°$ grid centered on each NCDC station. The 3-hourly data are taken to be piece-wise constant from one analysis time to the next for association with the hourly gauge data; for instance, the 1800 UTC reanalysis values are associated with hourly rainfall rates at 1800, 1900, and 2000 UTC. Interpolation of the reanalysis data onto the $1° \times 1°$ grid captures large-scale atmospheric features from the reanalysis in the vicinity of the observed rainfall and removes some of the smallest-scale features. Table 1 lists the NARR variables used. They include variables representative of moisture availability (i.e., surface temperature T_s, dewpoint temperature T_d, boundary layer specific humidity Q_m, and RH), vertical instability [i.e., CAPE, CIN, and 0–6-km vertical wind shear (S06)], and advective processes (i.e., the wind direction ϕ). Where variables involve averaging in their formulation, the interpolation is performed first, followed by the calculation step. This collection of variables has the potential to identify the relative importance regionally and seasonally of moisture availability, local instability, and advective processes.

Several issues influence the quality of NARR atmospheric profiles positively and negatively (Tippett et al. 2014; Allen et al. 2015a). Gensini et al. (2014) and Baldwin et al. (2002) identified moisture biases in the midlayers, particularly over the western Great Plains associated with mixing from the shallow convective scheme. West et al. (2007) identified areas of overly moist surface profiles. On the other hand, wind profiles from reanalysis above the boundary layer are considered

TABLE 1. List of variables and their units included in the analysis.

Name	Unit	Variable
I, $I^+_{p,V}$	mm h^{-1}	Rainfall intensity
T_s	°C	Surface temp (2 m)
CAPE$_s$	J kg^{-1}	Avg surface convective available potential energy (CAPE)
CIN$_s$	J kg^{-1}	Avg surface convective inhibition (CIN)
$T_{d,s}$	°C	Dewpoint temp at 2 m
RH$_s$, RH$_{70}$	%	Relative humidity at 2 m and 70 hPa above ground
S06	m s^{-1}	Wind shear between 10 m and 6 km above ground
Q_m	g kg^{-1}	Avg boundary layer specific humidity
ϕ_s, ϕ_{70}	m s^{-1}	Meteorological wind direction at 10 m and 70 hPa above ground

to be equivalent with rawinsonde profiles (Allen and Karoly 2014; Gensini et al. 2014), and the assimilation of observed rainfall as latent heat profiles may contribute to an improved product. This quality has been illustrated in examination of convective variables and other common parameters that suggest thermodynamic atmospheric properties are generally well represented (Mesinger et al. 2006; Gensini et al. 2014). Finally, by matching the NARR products with rainfall gauge data, rather than rainfall reanalysis products, we make use of a ground-observed and more reliable rainfall measurement (Bukovsky and Karoly 2007).

3. Methods

Calculation of conditional distributions and their analysis

We define *rainy hours* at each station as those hours when the station precipitation and the reanalysis surface temperature are both positive, and restrict our analysis to rainy hour precipitation intensity, where by intensity we mean hourly rainfall rate. There is no analysis of rainfall amounts accumulated from one hour to the next. Requiring positive surface temperature restricts the analysis almost exclusively to surface liquid precipitation. We abbreviate the condition $I > 0$ and $T_s > 0$, as I^+. For any reanalysis variable V, the distribution of rainy hour precipitation intensities conditional on the value of V is denoted $p(I \mid I^+, V)$ and is computed as in Lepore et al. (2015) by binning rainy hour precipitation intensities according to the corresponding value of the variable V. We use 20 bins, equally spaced over the range of V. For instance, the distribution of rainy hour precipitation intensity conditional on surface temperature, $p(I \mid I^+, T_s)$, is computed using 20 equally spaced bins over the range of T_s from 0° to 40°C. The p-percentile values for each of these 20 conditional distributions are computed for $p = 0.75, 0.8, 0.85, 0.9, 0.95, 0.98, 0.99, 0.995, 0.998, 0.999$. The percentile values of the conditional distribution $p(I \mid I^+, V)$ depend on the percentile probability p and the variable V and are denoted as $I^+_{p,V}$. In the case of the variables CAPE$_s$, CIN$_s$, and Q_m, the natural logarithm is applied to the variables [in the case of CIN, which has negative values, we use $-\ln(-\text{CIN}_s)$]. The other variables are not transformed. Bivariate conditional distributions $p(I \mid I^+, V_1, V_2)$ are calculated in the same way by binning rainy hour precipitation rates conditional on the values of the two variables V_1 and V_2 and again using 20 equally spaced bins for each variable. The percentiles of the bivariate conditional distributions are denoted I^+_{p,V_1,V_2}.

The dependence of the distribution of rainy hour precipitation rate on the variable V is shown by plotting the conditional percentiles $I^+_{p,V}$ as a function of V, and this graph is referred to as a *quantile plot*. In several cases, the conditional percentiles have a log-linear dependence on the variable V. This dependence is summarized by the slope s_p, which is found by fitting a linear regression of the form

$$\ln I^+_{p,V} = s_p V + \text{constant}, \tag{1}$$

which linearly relates the natural logarithm of the conditional percentile with the variable V over a range of values of V for which the linear assumption is adequate. For untransformed variables, Eq. (1) describes conditional percentiles that scale exponentially with the atmospheric variable; for logarithmically transformed variables, the conditional percentiles scale with a power of the atmospheric variable. The dependence of the slopes s_p on the percentile probability p is shown in *slope plots*. The dependence of the bivariate conditional distribution on V_1 and V_2 is summarized in a similar manner by fitting, for each p, a multiple linear regression of the form

$$\ln I^+_{p,V_1,V_2} = s_{p,1} V_1 + s_{p,2} V_2 + \text{constant}. \tag{2}$$

4. Results

a. *Frequency of rainy hours and convective rainy hours*

The annual frequency of rainy hours in Fig. 1 shows that rainy hours are most frequent in the northern part of the West region along with the East and Northeast regions. Figure 2 shows the annual and seasonal frequency of rainy hours for the eight regions. The annual CONUS frequency of rainy hours is ~6%, with regional values ranging from a low of 2% for the Southwest to a

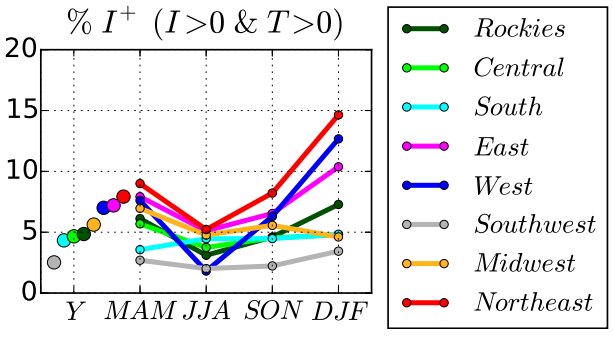

FIG. 2. Annual (Y; circles) and seasonal (MAM–DJF; lines) regional frequencies of rainy hours (%). Regions are indicated by the color given in the legend.

high of 9% for the Northeast. Seasonality is strongest in the coastal and eastern regions (Northeast, West, and East), with the most rainy hours in winter and the fewest in summer. The frequency of rainy hours in the Central, Midwest, South, and Southwest regions shows substantially less seasonality. Spring and fall values in each region are generally similar to the annual values.

The simplest characterization of rainfall type used here is $\mathrm{CAPE}_s \geq 1\,\mathrm{J\,kg^{-1}}$, (denoted CAPE^{+1}). The fraction of rainy hours with CAPE^{+1} is presented in Fig. 3 and can be interpreted as a zero-order indicator of the frequency of convection. The annual fraction of rainy hours with CAPE^{+1} is greatest in the South (90%) and lower frequencies are found for the Southwest (70%), East, Central, Rockies, and West (≈60%), and about 50% for the Northeast and Midwest (Fig. 3a). All regions except the West show strong seasonality with rainy hours, with CAPE^{+1} being most common in summer (100% of the South rainy hours) and least common in winter.

We consider also three multivariate characterizations of rainfall type that have been applied in the literature to convective or severe convective storms (Table 2). Allen et al. (2011) used linear discriminant analysis to separate between severe convective storms [defined as those producing 2 cm+ diameter hail, 50 kt or greater winds (where $1\,\mathrm{kt} = 0.51\,\mathrm{m\,s^{-1}}$), or any tornado] and non-severe convective storms, while other discriminants have sought to identify "significant" severe convection [responsible for 5 cm+ diameter hail, 65 kt or greater winds, and F2+ tornadoes; Brooks et al. (2003); Allen et al. (2011)]. The product of CAPE and S06 or S06 raised to a power greater than one is common to many of

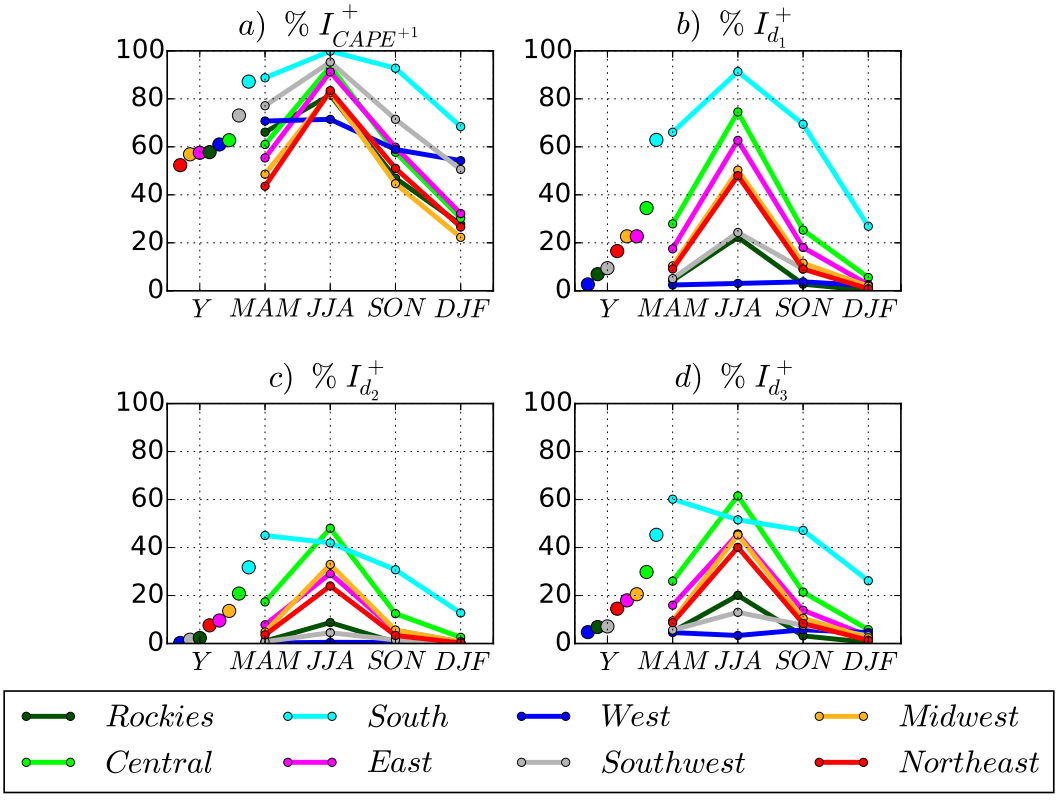

FIG. 3. Annual (Y; circles) and seasonal (MAM–DJF; lines) fractions of convective rainy hours as defined by (a) CAPE > 1 and discriminants (b) d1, (c) d2, and (d) d3. Regions are indicated by the color given in the legend.

TABLE 2. The three multivariate discriminants of convectivity.

Name	Discriminant
d1	$(\text{CAPE})(\text{S06}) + 23.3Q_m > 5667$
d2	$(\text{CAPE})(\text{S06}) > 10\,000$
d3	$(\text{CAPE})(\text{S06}^{1.67}) > 25\,000$

these severe thunderstorm discriminants (Marsh et al. 2007; Trapp et al. 2007). The first discriminant, denoted d1, depends on the product of CAPE, S06, and Q_m and is adapted from the linear discriminant of Li and Colle (2014), which was developed to identify the environmental conditions favorable to convective storms regardless of severity using radar observations and convective precipitation data for the northeast United States. The other two discriminants, denoted d2 and d3, depend only on CAPE and S06 and were used in Marsh et al. (2007) and Allen and Karoly (2014), respectively, to characterize severe thunderstorm environments.

The annual and seasonal fractions of rainy hours satisfying d1–d3 are shown in Figs. 3b–d. The three discriminants give a mostly consistent ordering of the annual fraction of convective rainy hours with the highest values in the South and Central regions; followed by the Midwest, East and Northeast regions; and finally the Southwest, Rockies and West regions. The highest fraction of convective rainy hours occurs in summer for all discriminants and regions except the South. Convective rainy hours in the South region are most frequent in summer according to CAPE^{+1} and d1, but in spring according to the two discriminants d2 and d3, which do not include moisture Q_m. The West region shows little seasonality according to any of the three discriminants. Overall, the convective rainy hours are most frequent according to d1 and least frequent according to d2.

b. *Univariate dependence of rainy hour rainfall intensity on environment*

The distribution of rainy hour rainfall rates conditional on the surrounding environment is characterized by the dependence of the conditional percentiles $I^+_{p,V}$ on the value of the reanalysis variable V in Fig. 4. Starting with T_s (Fig. 4, first row), in most of the regions the natural logarithm of the rainfall percentiles $\ln(I^+_p)$ shows an overall positive relationship with surface temperature T_s, indicating exponential sensitivity to surface temperature. The slopes [see Eq. (1)] of the percentiles are shown in Fig. 5 and indicate slope values well below the CC rate (6.8% K^{-1}) for the lower percentiles ($p < 0.95$), which then increase and plateau at or just above the CC rate for the higher percentiles. This differing pattern of behavior shows the increasing sensitivity to temperature of higher quantiles of hourly rainfall intensities. The highest sensitivities are seen for the South, Central, Midwest, and Northeast regions, and the lowest for the West region. The surface temperature slope values are slightly lower than those in Lepore et al. (2015), but are overall similar in their shape and range of values.

The percentile plots for dewpoint temperature $T_{d,s}$ (Fig. 4, second row) display a more linear behavior than do the ones for surface temperature, with no inflection point. Percentiles for the West region show a much more linear scaling with dewpoint temperature than with surface temperature for percentile levels greater than 0.95. The slope values for dewpoint temperature are mostly at or slightly above the CC rate (Fig. 5; $T_{d,s}$), in contrast to those for surface temperature. The regional dependence of the slopes is somewhat less for dewpoint temperature (excluding the West and Rockies regions) than for surface temperature, a finding that may be relevant for statistical modeling.

Percentiles of rainy hour intensities conditional on CAPE (Fig. 4, third row) show threshold behavior with $\ln(I^+_p)$ scaling linearly with $\ln(\text{CAPE}_s)$ for values of CAPE greater than $50\,\text{J}\,\text{kg}^{-1}$, except for the West region, where there is little dependence on CAPE. The slope values for CAPE in Fig. 5 are mostly in the neighborhood of 0.2; this value is lower than the theoretical value of 0.5, which comes from the idealized scaling of updraft velocity with the square root of CAPE. Values lower than 0.5 are expected in nonidealized conditions (Singh and O'Gorman 2014; Lepore et al. 2015). There is some indication of a reduced sensitivity to CAPE at higher percentiles in the Midwest and East. The contrasting negative relationship between convective inhibition CIN_s and rainfall is therefore expected given it parameterizes resistance to atmospheric destabilization. In our analysis, where we consider rainy hours only, higher CIN_s values do not completely inhibit rainfall, but rather work as a retardant to the development of convection; in the environment preceding convection, greater CIN_s allows for a stronger moisture convergence before convective initiation and, thus, can promote higher rainfall intensities when convection does develop. In the case of nonrainy hours, CIN_s can preclude convective processes and cloud formation altogether. The negative relationship is found throughout the CONUS but varies in degree; the corresponding slope plots (Fig. 5; CIN_s) do not depend on the percentile levels, but mostly on the geographic location; the highest negative slopes being for the interior western United States (Rockies and Southwest), and the lowest values for the South and West, suggesting that the different range of slope values seen in Fig. 5 for

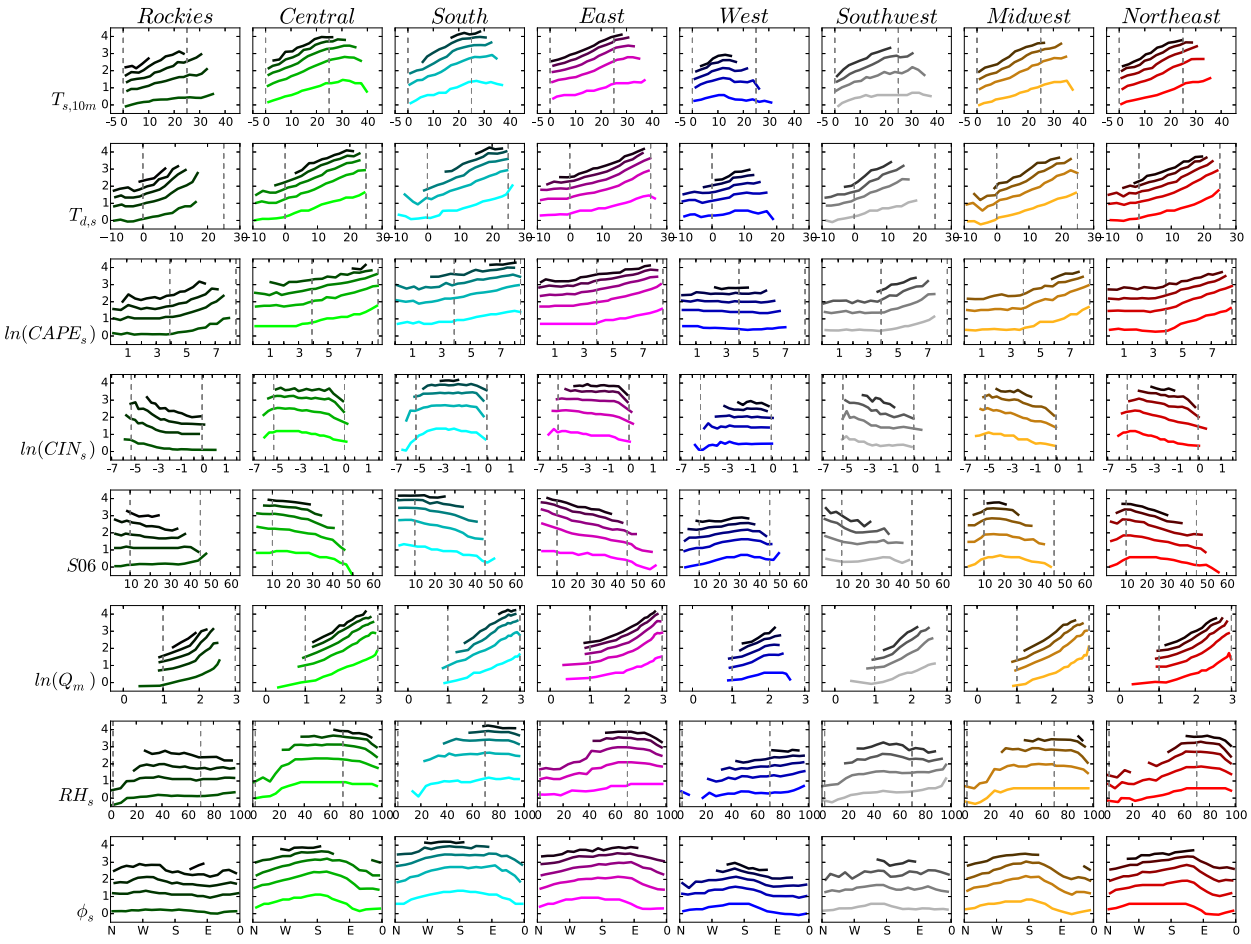

FIG. 4. Percentiles of the regional distribution of rainy hour rainfall intensity conditional on reanalysis variables. Each row corresponds to a reanalysis variable (labeled on the left), and each column to a region (labeled at the top). The natural logarithms of the conditional percentiles $\ln(I^+_{p,V})$ (y axis) are plotted as a function of the reanalysis variable V (x axis) for the percentile levels $p = 0.75, 0.95, 0.99, 0.998$, and 0.9995 with lighter colors corresponding to lower percentiles and darker colors to higher percentiles. The two gray vertical dashed lines in each plot (except surface wind direction ϕ_s) show the range of values used to calculate the slopes in Fig. 5.

CIN_s reflects the differing degree of dependence of convective rainfall on CIN within the United States.

In all regions east of the Rockies, rainy hour precipitation intensity has a clear overall negative relationship with S06 (Fig. 4, fifth row), a quantity that appears in the linear discriminants d1–d3 for convective and severe convective storms. The conditional percentiles show either little sensitivity or positive sensitivity (Midwest and Northeast regions) to S06 when its values are less than about $10\,\mathrm{m\,s^{-1}}$. There is a linear regime for values of S06 between 10 and $45\,\mathrm{m\,s^{-1}}$ where the Rockies region shows no clear slope, the West region shows a positive slope, and all other regions show a negative relation between rainfall percentiles and S06. An explanation for this behavior is that increased S06 can reflect an increased 6-km wind velocity, which has the consequence of a faster cloud or storm motion, which would reduce the residence time over a gauge of any rain-bearing cloud. Another possible explanation is that convection with insufficient $CAPE_s$ will be unable to sustain its updraft in the presence of increasing entrainment from midlayer wind shear. This hypothesis is evaluated in the next section when we consider the combined effect of CAPE and S06 on the rainfall process. In the corresponding slope plots (Fig. 5; S06), the negative relationship between S06 and $\ln(I^+)$ is variable but fairly robust in regions east of the Rockies.

The sensitivities of rainy hour rainfall intensity to boundary layer specific humidity Q_m and surface relative humidity RH_s are quite different. The overall relation of boundary layer specific humidity Q_m with rainfall rate is positive in all regions, at almost all percentile levels (Fig. 4, sixth row). The slope plots [Fig. 5, $\ln(Q_m)$] show that the transformation rates of specific

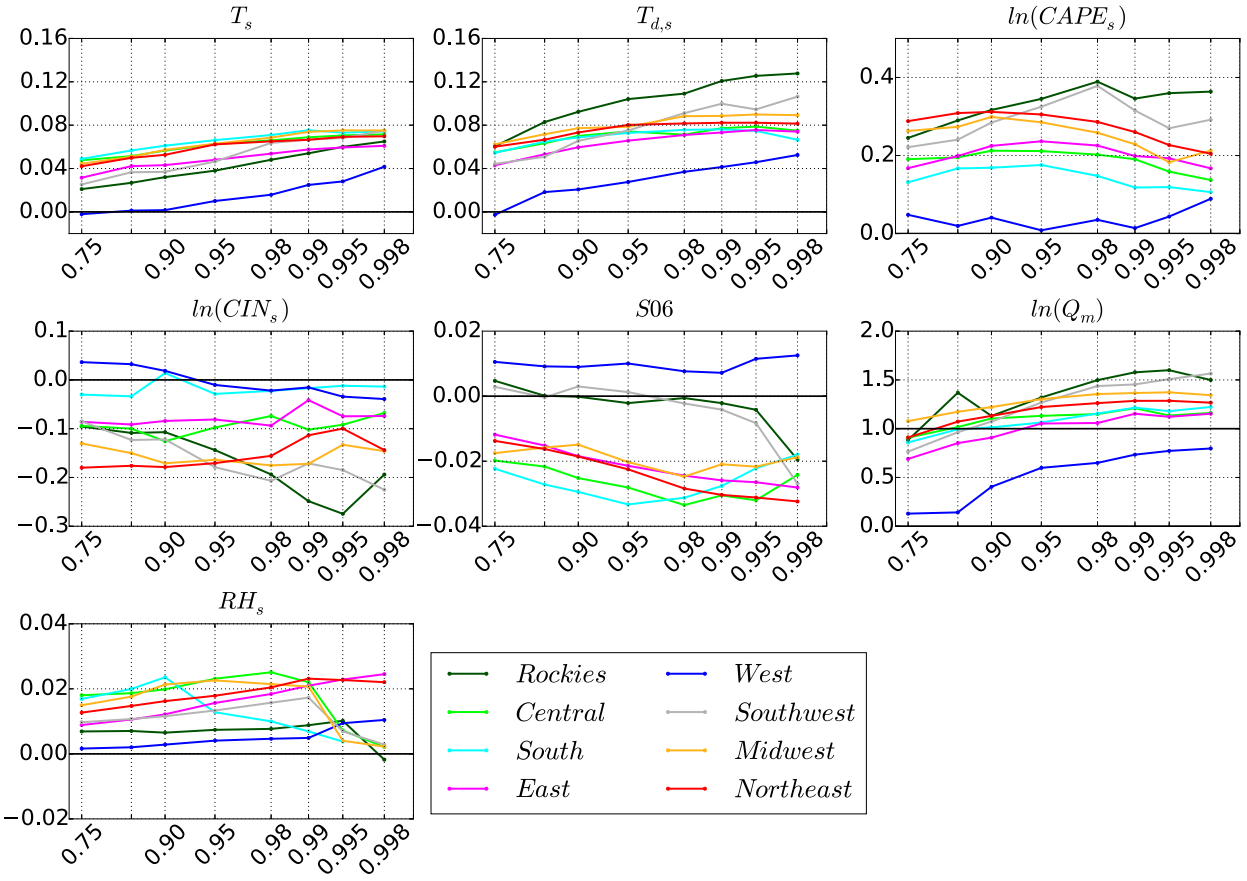

FIG. 5. The vertical axis reports the slope values [s_p in Eq. (1)] of the linear regression calculated on the quantile plots presented in Fig. 4. The horizontal axis is for percentile levels; the titles indicate the variables considered in the panel. The black horizontal lines in T_s, T_d, $\ln(\mathrm{CIN}_s)$, and S06 highlight the zero-slope line, in $\ln(Q_m)$, the one-slope line.

humidity into rainfall intensity are on the order of 1 for percentile probabilities between $p = 0.75$ and 0.90 for all regions except the West. Percentile slopes increase for all regions for percentile probabilities greater than 0.95, and all slopes exceed 1 for the highest percentiles except in the West region. Slope values greater than 1 indicate that moisture is added compared to the average available moisture for a region. This additional moisture can be due to stronger moisture convergence, and in particular it could be induced by other water/energy conversion mechanisms (i.e., CAPE). In addition, RH_s is related to surface temperature and available moisture, but has a less straightforward relation with rainy hour rainfall rate, except in the West region, where it is an overall positive and mostly linear relation. For low values of RH_s, most regions show a positive relation with rainy hour rainfall rate, and a negative relation for high values of RH_s. Overall, RH_s shows weaker relationships with hourly rainfall intensity compared to other measures of temperature and moisture, such as $T_{d,s}$ and $\ln(Q_m)$.

Finally, the relationship between the wind direction ϕ and hourly rainfall intensities (Fig. 4, eighth row) is used to highlight the preferential wind direction, or the lack of wind (0 wind identifies no wind), for more intense rainfall occurrences in each region. Because of the shape of these relationships, slope values were not calculated for this quantity. The synoptic flow patterns associated with prefrontal warm-air advection and postfrontal wind regimes from the west or south are preferential for rainfall in most regions. Regional variations can also reflect the climatological wind direction of higher moisture content, favoring southerly flow in the central plains, South, and Midwest for intense rainfall, or southeasterly flow (Northeast and East).

Overall, hourly rainfall intensity in the West region displays different sensitivities compared to the other regions. Rainfall percentiles over the West region do show clear sensitivity to dewpoint temperature T_d, S06, and boundary layer moisture Q_m, but the slope values (Fig. 5) are substantially different from those of the other regions, and in the case of S06, the sign of the slope

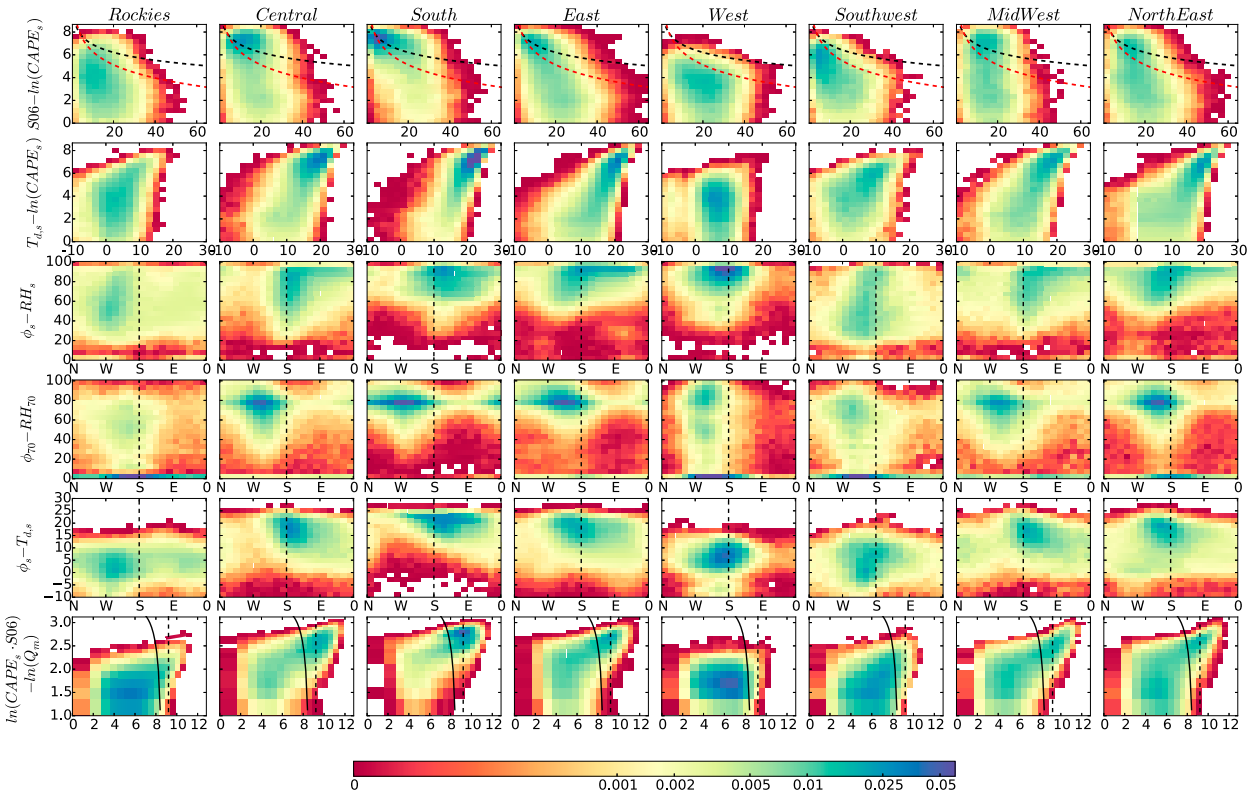

FIG. 6. The bivariate distribution of environments V_1 and V_2 conditional on rainy hour occurrence and $\mathrm{CAPE}_s > 1$, denoted $p(V_1, V_2 \,|\, I^+, \mathrm{CAPE}^{+1})$. Each column corresponds to one of the eight regions, labeled at the top. Each row corresponds to a different pair of variables, V_1 and V_2, given in the leftmost label and corresponding to the horizontal and vertical axes, respectively [i.e., in the first row, the label S06 − ln(CAPE$_s$) indicates that S06 corresponds to the x axis and ln(CAPE$_s$) to the y axis]. White areas correspond to values of V_1 and V_2 that do not occur during rainy hours with CAPE^{+1}, while red and blue areas correspond to values of V_1 and V_2 that occur rarely and most commonly, respectively. In the first row, the dashed lines show the linear discriminants d2 (black) and d3 (red). Dashed lines in the third to fifth rows identify the southerly direction. In the last row the solid line identifies the discriminant d1 and the black dashed line corresponds to d2.

is different. The distinct dependence of the West region rainfall rate on the environment is consistent with assessments that intense rainfall processes in this region are heavily driven by nonlocal processes such as atmospheric rivers (e.g., Steinschneider and Lall 2015), reflected by the sensitivity to boundary layer moisture, the positive relation with vertical wind shear, and preferential wind directions during intense rainfall from the west and southwest.

Repeating these analyses at the seasonal time scale reveals that the relationships to atmospheric variables in fall (SON) and spring (MAM) are very similar to the results found when using the entire year. In contrast, winter (DJF) and summer (JJA) show considerable differences, with the rainy hour rainfall rate being insensitive to ln(CAPE) in winter. The slopes for T_d and Q_m in winter are closer to the annual case. For the summer months, the ln(CAPE) slope values are similar to those shown for the entire year, and the West region appears to have slopes comparable to the other regions, as well. Repeating the analysis on six 5-yr subsets confirms that the relationships for rainfall percentiles with atmospheric variables are robust with no significant change over the past 30 yr.

c. *Bivariate dependence of rainy hour rainfall intensity on environment*

We first consider the bivariate distributions of atmospheric variables V_1 and V_2 conditioned on rainfall occurrence and CAPE^{+1}, denoted $p(V_1, V_2 \,|\, I^+, \mathrm{CAPE}^{+1})$ and displayed in Fig. 6, for various choices of V_1 and V_2. This quantity shows the joint frequency of environments during rainy hours with $\mathrm{CAPE}_s > 1$. The joint distribution of S06 and ln(CAPE$_s$) reveals notable regional features in the source of precipitation (Fig. 6, row 1). In the South, environment occurrence during rainy hours with CAPE^{+1} is concentrated along or above the discriminant thresholds, as reflected by the greater fraction

of rainfall events in blue, which is in line with the convective characteristics of the rainfall process in this region. The Central, Midwest, and Southwest regions also show a considerable proportion of rainfall linked to the environmental phase space corresponding to severe convection. In the West, little to none of the rainfall is found within severe convection conditions, with the majority of the rainfall distribution located in a part of environmental phase space that rarely produces convection. This lack of dependence on convection for producing the majority of the rainfall in the region is consistent with the observation that the main rainfall source for the West is via moisture advection and atmospheric rivers, or large-scale orographic uplift (Ralph et al. 2005, 2006; Smith et al. 2010; Steinschneider and Lall 2015, and reference therein), and is consistent with the weak dependence on local atmospheric states found for the univariate case. A relatively narrow and concentrated area of *blue* (high) frequency for the South region is also evident for the joint probability of [$T_{d,s}$, $\ln(\text{CAPE}_s)$] (Fig. 6, row 2). For the West region, the lack of dependence on convective processes is further emphasized by the sensitivity to $T_{d,s}$ but not CAPE_s. The other regions considered show a similar shape in joint [$T_{d,s}$, $\ln(\text{CAPE}_s)$] probability phase space, as well as comparable occurrence values.

In addition to parameters typically related to convection, rainfall processes can be also related to the advection of moisture at various levels in the atmosphere. These can be visualized by considering variables describing moisture (i.e., RH and T_d) and the meteorological wind direction ϕ at 10 m (surface) and 70 hPa above ground (Fig. 6, rows 3–5). The modulations of the regional rainfall process by surface moisture advection is visualized using the joint distribution of (ϕ_s, RH_s), and identifies higher rainfall occurrence across a range of conditions (Fig. 6, rows 3). Predominantly, east of the Rockies, moisture advection is associated with south-to-southeasterly flow. The Southwest displays much lower RH values, and for the West, we identify a very localized regime for rainfall production, which corresponds to high RH values and S-to-SSW winds, which is consistent with the prevailing winds during atmospheric river events (Steinschneider and Lall 2015).

At 70 hPa above ground (Fig. 6, row 4), the majority of the rainfall is linked to the southwesterly-to-westerly wind direction, associated with the large-scale flow patterns. For the West, Southwest, and Rockies, the wide distribution over both RH and ϕ values suggests that the rainfall process is less likely to originate from a single preferential flow pattern, perhaps reflecting a reduced dependence on synoptic-scale systems, in contrast with the behavior over the Central, South, East, and Northeast, and to a lesser extent the Midwest, where rainfall occurrence strongly responds to increasing RH values and prevailing SW-to-W winds, suggesting a strong synoptic contribution.

The ϕ_s versus $T_{d,s}$ plots resemble the (ϕ_s, RH_s) depiction (Fig. 6, row 5), but add an additional piece of information: the temperature of the advected moisture [considering $T_d \approx T$ for $T < 22$; see Lepore et al. (2015)]. The codependence on temperature and ϕ_s is very pronounced for the majority of the eastern regions, but is less prevalent in the western regions, as identified in the univariate case.

Finally, we examine the joint behavior of $\ln[(\text{CAPE})(\text{S06})]$ and $\ln(Q_m)$ and its effect on rainfall occurrence; these three variables are used in the discriminant targeting primarily convection (d1; Table 2, Fig. 6, row 6). The joint behavior of these variables suggests the overall shape of the distribution can be split into two parts, below and above $\ln[(\text{CAPE})(\text{S06})] \approx 7$; in the latter case, I^+ shows a positive relationship between $\ln(Q_m)$ and the product of the other quantities. This feedback is of particular interest and in line with the results presented in the univariate section; higher Q_m values (which ultimately correspond to higher rainfall intensity values) occur when $\ln[(\text{CAPE})(\text{S06})]$ values are high, and when combined with stronger updraft velocities and organized storm modes, drive moisture convergence and the higher precipitation transformation rates seen in Fig. 5. Again, the majority of rainfall for the South is located in the convective region, whereas in the West rainfall occurrence is nearly exclusively below both thresholds.

This set of figures confirms the strong differences in rainfall properties between the eastern United States and the western part of the continent, in contrast with a more moderate *regionality* of precipitations over the eastern United States. An equivalent analysis performed using rainy hours with $\text{CAPE}^{<1}$ (not shown) gives similar results for (ϕ, RH) and (ϕ, $T_{d,s}$) joint analyses. The only noticeable difference is a more limited temperature range for $T_{d,s}$, as would be expected with negligible values of CAPE.

Seasonality is also of interest in precipitation processes, and the joint distributions of environments for rainy hours with $\text{CAPE}_s > 1$ in winter (DJF) and summer (JJA) are presented in Fig. 7. In winter there are fewer hours with $T > 0$ and $\text{CAPE}_s \geq 1\,\text{J kg}^{-1}$, and therefore, these results represent only part of the precipitation process that takes place during winter months, especially for regions where snowfall is important. For the winter months (Figs. 7a,c,e,g), environment occurrence during rainy hours with $\text{CAPE}_s > 1$ is confined below the severe weather discriminants for the Rockies,

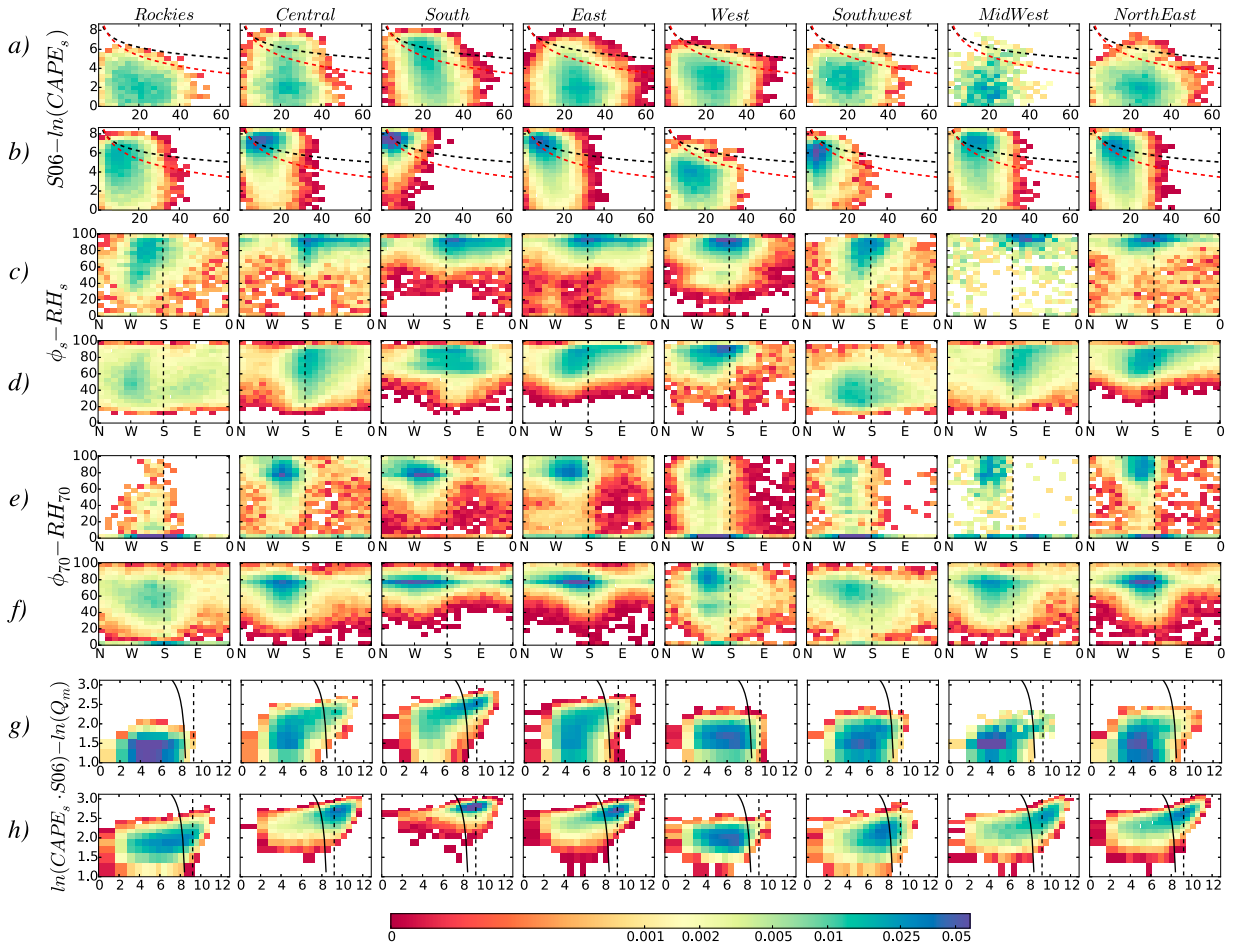

FIG. 7. As in Fig. 6, but for seasonal results: (a),(c),(e),(g) DJF and (b),(d),(f),(h) JJA. In (a) and (b), the dashed lines show the two discriminants d2 (black) and d3 (red). In the (c)–(f), the dashed line identifies the southerly direction. In (g) and (h), the solid line identifies the convective discriminant d1 and the dashed line corresponds to d2.

particularly for the West, and, to a lesser degree, for the Southwest, Northeast, and Midwest, reflecting the very low likelihood of encountering severe convection in the western United States during winter months; the opposite is true for the summer months, when much of the environment occurrence, especially for the eastern United States, happens in the convective or severe convective regimes (Figs. 7b,h). These differing patterns of behavior in winter and summer validate how representative this discriminant can be for identifying seasonality within severe convection.

Overall, winter precipitation occurrence appears to have a reduced dependence on the local atmospheric state, with Figs. 7a,g displaying less preferential rainfall areas compared to the whole-year analysis in Fig. 6. There is instead a pronounced dependence on the wind direction and moisture, with very distinct blue areas in the plots of Figs. 7c,e, reflecting the prevalence of frontal storms during this season. Summer precipitation occurrence, however, is well described using the local atmospheric conditions and thermodynamic parameters Figs. 7b,h. For the $\mathrm{CAPE}^{<1}$ case (not shown here), the winter results are very similar to the CAPE^{+1} case, whereas the sample size in summer is too small.

The previous figures explore how atmospheric variables are distributed during rainy hours with $\mathrm{CAPE}_s > 1$, which is influenced by the climatological distribution $p(V_1, V_2)$ as well. In Fig. 8, we show the likelihood of rainy hours conditional on the two variables V_1 and V_2 and $\mathrm{CAPE}_s > 1$. If the likelihood of rainy hours were independent of the environment, the values would be constant and equal to the regional likelihood of rainy hours. Figure 8 shows this analysis for two sets of variables, $[T_d, \ln(\mathrm{CAPE}_s)]$, and surface moisture advection (ϕ_s, RH_s); hatched grid points represent no significant difference from the regional likelihood of rainy hours. For $[T_d, \ln(\mathrm{CAPE}_s)]$, the likelihood of rainy hours does

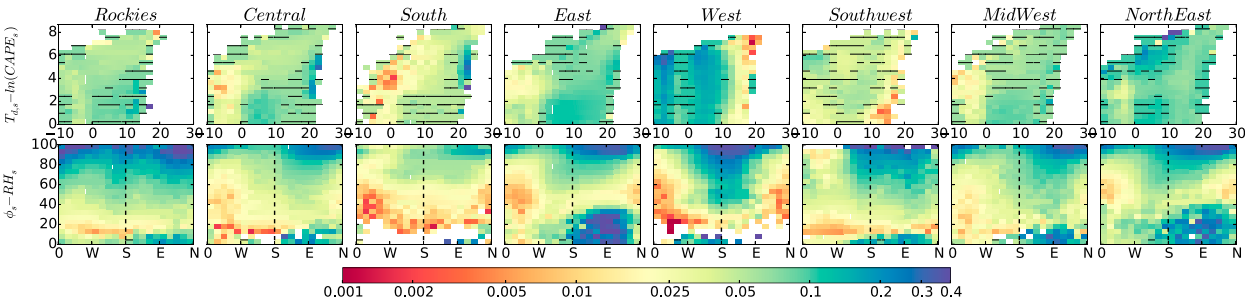

FIG. 8. The expected rainfall occurrence conditioned to a specific atmospheric state, $\%I^{+}_{V_1,V_2}$; hatched grid points represent no significant difference from the average regional value of $\%I^{+}$ (shown in Fig. 2). These results are for CAPE^{+1}.

not vary noticeably, staying within about 50% of the regional likelihood, and a relatively lower occurrence for $T_d < 0$. In comparison, in the second row of Fig. 8, for the variables (ϕ_s, RH$_s$), we find a large degree of variability. In particular, there appear to be different ranges of likely rainfall-producing states, corresponding to a rainy hours likelihoods greater than 20%. In all regions, RH$_s > 80\%$, almost independently of the wind direction, corresponds to a high probability of rainfall occurrence. The influence of wind direction is more noticeable when RH$_s < 80\%$, and represents specific flow directions associated with extratropical storms (and can reflect potential moisture advection) and their influence on rainfall occurrence. In the West, high rainfall occurrence is tied to SE-to-SW wind directions, typical of atmospheric rivers or moisture of a tropical origin, while for the Southwest, rainfall occurrence is consistent with the prevailing winds during the North American monsoon. Finally, we notice two "pockets" of high $\%I^{+}_{V_1,V_2}$ for the East and Northeast regions (a portion of which is not significant), a result of easterly prevailing winds mostly due to winter precipitation. This last set of results shows how ϕ has different explanatory power compared to the other thermodynamic and dynamic variables, capable of modeling the occurrence of rainfall.

d. *Multivariate conditional percentiles*

We extend the univariate results presented in Figs. 4 and 5, showing the dependence of rainy hour rainfall-rate percentiles on the environment to the multivariate setting and compute the conditional percentiles I^{+}_{p,V_1,V_2}. Based on the results presented in Fig. 5, where we show the coefficients of the univariate linear regression fitted to the quantile plots, we expect to see somewhat limited regional variability (especially for some variables, e.g., $T_{d,s}$) with most of the differences in the West region and the highest intensity values in the South. The results are presented in Fig. 9 for three pairs of variables: S06 and ln(CAPE$_s$), ϕ_s and $T_{d,s}$, and ln[(CAPE)(S06)] and ln(Q_m).

Starting from the first set in Fig. 9 [S06–ln(CAPE$_s$)], there is an increasing contribution from severe thunderstorms with increasing intensity (as we move left to right, from $p = 0.95$ to 0.999). Outside of the Rockies and the West regions, darker blues, and any of the colors in general, are located above the severe weather discriminant. This trend hold particularly for the Central and South regions, where the highest rainfall intensities ($p \geq 0.999$) are at or above the discriminant dashed lines. This result is also true for the third block of plots, ln[(CAPE)(S06)]–ln(Q_m), where both variables have an effect on the rainfall intensity. The relationship of intensity to moisture advection, shown in the ϕ_s–$T_{d,s}$ block, instead, reveals dependence mostly on $T_{d,s}$, with a vertical color gradient, whereas wind direction shows its strong effect on rainfall occurrence, similar to Fig. 6. Similar implications are found for the respective seasons (not shown).

The South displays overall higher intensity values (darker blue) than the other regions, while the West shows a negligible gradient, suggesting little dependence on the set of variables. The results shown in this last set of panels further suggest moderate regional dependence for the conditional intensity distribution, outside of the West region outlier, and to some degree the South.

The first set of Fig. 9 [S06–ln(CAPE$_s$)] confirms some of the conclusions drawn in the univariate case. In particular, the negative slopes found in row 5 in Fig. 4 (S06), which we explained as being due to insufficient CAPE$_s$, are unable to sustain updrafts in the presence of increasing wind shear; by looking at the relationships between log-intensity versus S06 and ln(CAPE$_s$), we notice how the highest intensities (blue/green color) are those related to higher CAPE values, which becomes less frequent with increasing shear (hence the *tilted* shape of the green/yellow areas in Fig. 9). Therefore, the highest intensities are able to develop when there is sufficient CAPE to sustain updraft during high wind shear, which is however not often found for high values of shear.

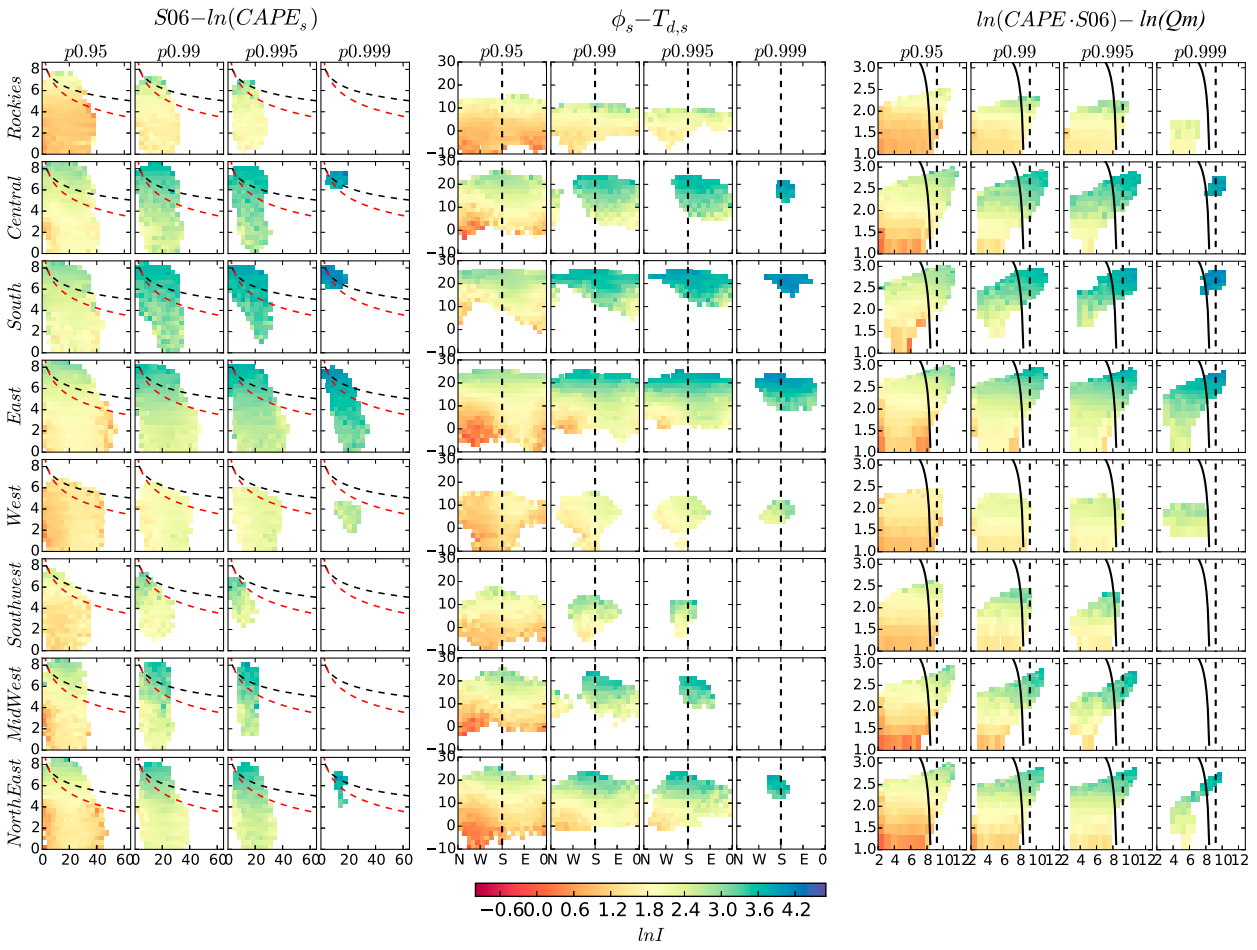

FIG. 9. Natural logarithms (colors) of the rainy hour rainfall rate percentiles with $\mathrm{CAPE}_s > 1$ and conditional on [S06, $\ln(\mathrm{CAPE}_s)$], (ϕ_s, $T_{d,s}$), and $\{\ln[(\mathrm{CAPE})(\mathrm{S06})],\ \ln(Q_m)\}$. The percentile levels shown are $p = 0.95$, 0.99, 0.995, and 0.999. In the first set of panels [S06, $\ln(\mathrm{CAPE}_s)$], the dashed lines show the two discriminants, d2 (black) and d3 (red). In the second set (ϕ_s, $T_{d,s}$), the dashed lines identify the southerly wind direction. In the last set $\{\ln[(\mathrm{CAPE})(\mathrm{S06})],\ \ln(Q_m)\}$, the solid line identifies the convective discriminant, d1, and the black dashed line corresponds to d2.

We evaluate the coefficients of the multivariate regression in Eq. (2) to quantify the best set of regressors and their relative efficiency in describing the intensity process. The results of various variable combinations are presented in Fig. 10. We first inspect the coefficients for [$T_{d,s}$, $\ln(\mathrm{CAPE}_s)$]; this combination was also used in Lepore et al. (2015), and our results, as in the univariate case, are in line with the previous analysis. The coefficients for CAPE are half of those found in the univariate case (Fig. 5), going from about 0.3 to 0.15, and decreasing for percentiles $p > 0.9$ (Fig. 10, row 1). Regional variability of the coefficients is also more limited compared to the univariate case, as seen in $T_{d,s}$. Similar results are obtained where in place of dewpoint temperature we use specific humidity, $\ln(Q_m)$ (Fig. 10, row 2). The thermodynamic components of these two regressions, $T_{d,S}$ and $\ln(Q_m)$, display similar ranges of coefficients as in the univariate case. In both cases the quantitative evaluation of regressions via the percentage of the explained sum of squares (%ESS) is very high, with a slightly higher value from using $\ln(Q_m)$. For both combinations, both regressors are highly significant (with p values $\ll 0.05$), and with about 70% of the total %ESS due to the thermodynamic component. For the West region, %ESS values are lower and the coefficient of $\ln(\mathrm{CAPE}_s)$ is not significant (p values ≈ 0.1).

These regressions represent two pathways through which changes in atmospheric temperature can affect the rainfall process; while very relevant to the process, they exclude other types of processes not strictly related to the local temperature (i.e., S06, U, and V), which may be relevant to the description of the regional rainfall process. To analyze the contributions of other factors, we consider alternatives (Fig. 10, rows 3 and 4) that

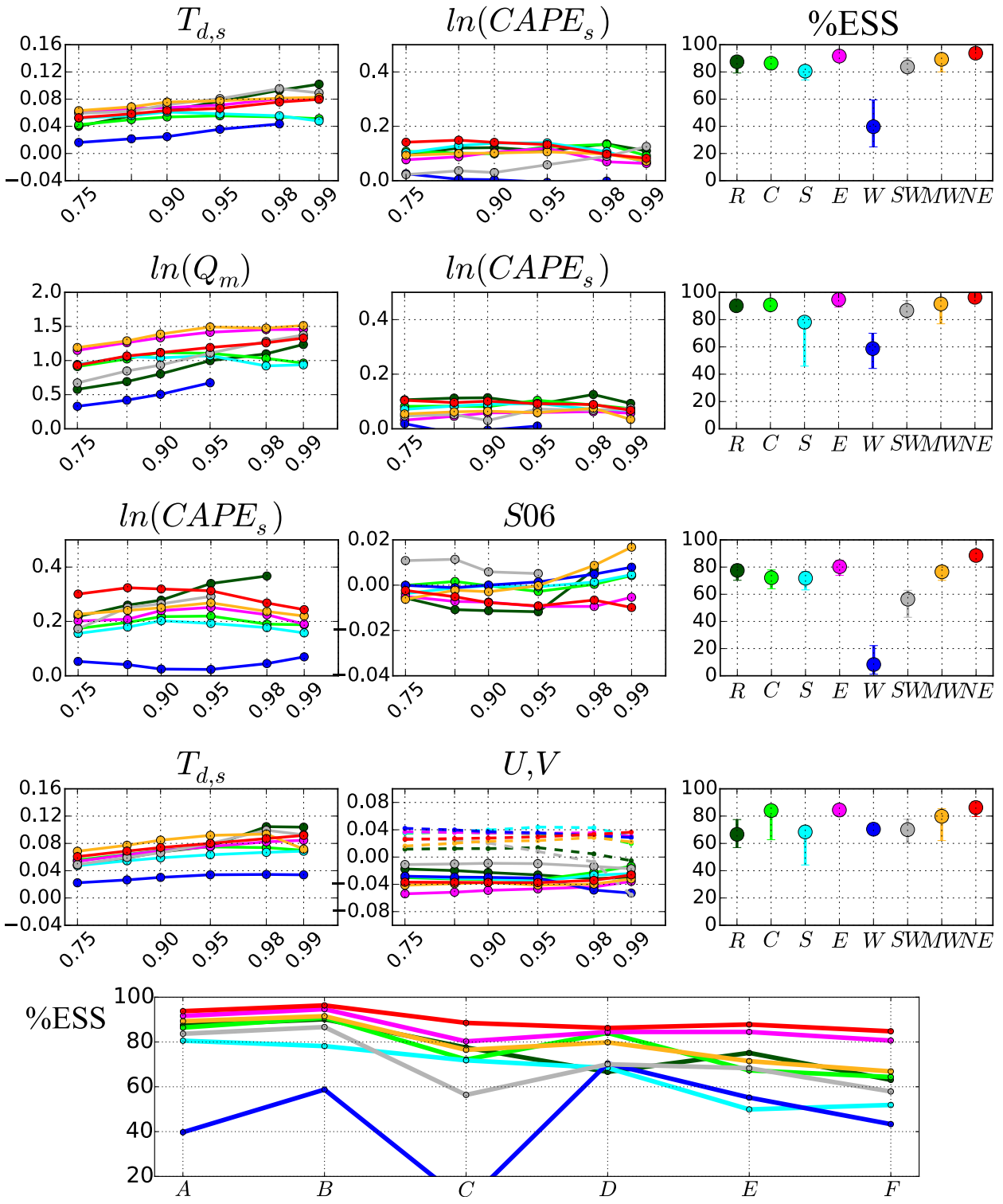

FIG. 10. The first two columns show the coefficients of the regressions between log-intensity percentiles, $\ln(I_p^+)$, and two or more regressors for a range of percentile levels (horizontal axis). The title indicates the regressor. In the fourth row, second column, the dashed lines are for U, whereas the solid lines are for V. The last column shows %ESS, with different colors for different regions. The bottom panel shows the %ESS for all considered regression models: A for [$T_{d,S}$, ln($CAPE_s$)], B for [ln(Q_m), ln(CAPE$_s$)], C for [$T_{d,S}$, ln(CAPE$_s$)], D for ($T_{d,S}$, U, V), E for [$T_{d,S}$, ln(CAPE$_s$), S06], and F for [ln(Q_m), ln(CAPE$_s$), S06]. Here R, C, S, E, W, SW, MW and NE are short for the Rockies, Central, South, East, West, Southwest, Midwest and Northeast regions, respectively.

match one of the previous variables, ln(CAPE$_s$) or $T_{d,s}$, with other regressors. Both regressions show lower total %ESS compared to the previous cases. The S06 coefficients are significant for the regions east of the Rockies only, and where significant, the S06 contribution to %ESS is small (<10%). The U and V coefficients are significant in all regions (p value < 0.05). In particular, in the West region, the meridional wind contributes a third of the total %ESS.

Finally, we compare the %ESS for these four models and include two other trivariate regressions: [$T_{d,s}$, ln(CAPE$_s$), S06] and {ln[Q_m, ln(CAPE$_s$), S06]}. We note that adding a third component to the different models generates a different set of conditional quantiles (i.e., $I_{p,T_{d,s},\mathrm{CAPE}_s}$ is different from $I_{p,T_{d,s},\mathrm{CAPE}_s,\mathrm{S06}}$). Within the last two trivariate models, S06 is a significant regressor for the eastern United States only, and about 90% of the total %ESS is due to the first two variables.

In summary, we confirm the importance of including both a thermodynamic and a dynamic variable in the description of the rainfall intensity process, for most of the regions in the United States. For the West, the best results are given by considering percentiles conditional on $T_{d,s}$ and the U, V wind components. The addition of a third regressor for the other regions appears to add little explanatory power to the regression and results in an overall less powerful model.

5. Conclusions

We have analyzed the dependence of high percentiles of hourly rainfall rate (intensity) on relevant atmospheric variables, using hourly gauge rainfall data and atmospheric quantities from reanalyses. This investigation extends the approach of relating the rainfall process and intensity to the environment by including a wider range of thermodynamic and meteorological variables, providing additional insight into the large- and regional-scale atmospheric contributions to the rainfall process. In addition, the consideration of common variables has allowed validation of previous results obtained using an alternative reanalysis over a more limited region, further supporting the statistical robustness of those findings (Lepore et al. 2015).

Two sets of analyses were considered: (i) the relationships of the hourly rainfall intensity conditioned on atmospheric drivers and (ii) how these drivers modulate the occurrence of the rainfall process. The thermodynamic variables CAPE, T, T_d, and ln(Q) were confirmed as being among the most important variables in the description of the rainfall intensity process and its extremes. Moreover, one of the key results for most regions of the United States is the need to consider both thermodynamic and dynamic variables for a complete description of the rainfall intensity process. A third regressor added little information to our regression model, and other variables such as ln(CIN), S06, and U and V identified more subtle properties of the regional rainfall intensity and occurrence process.

The regional variability of the relationships between rainfall intensity and atmospheric drivers is moderate east of the Rocky Mountains, while the western United States has relatively unique features. In this analysis, we find no strong relation in the West of local thermodynamic and dynamic properties with rainfall intensity, whereas moisture advection plays a dominant role. In contrast, the occurrence of rainfall has a strong regional signature. The differences observed in Figs. 6 and 7 can be used to extrapolate the major drivers of the regional properties of the precipitation process in the CONUS. These results suggest the possibility of consolidating the eight regions in three macroregional behaviors. The first macroregion encompasses the eastern regions (Midwest, Northeast, Central, East, and South), which show similar seasonal convective climatology, with the South displaying the highest values. The second region includes the Southwest and Rockies, which have very similar seasonality and are found in the middle of the regional range. Finally, the West appears to form a macroregion of its own at the other tail of the distribution.

These findings indicate some of the challenges in constructing global or even CONUS-wide statistical rainfall models. A single approach is not appropriate for describing these processes when exploring the relationships to the climate system, particularly for the West Coast of the United States.

Our approach reveals the utility of combining a variety of information in a simple image that encapsulates the rainfall process, as seen in Figs. 6–9. Furthermore, we couple this analysis with established linear discriminants to identify the contributions of specific weather states (i.e., nonconvective, convective, and severe convective) to the yearly and seasonal rainfall regimes for the whole CONUS. Our approach represents a novel and compact methodology for looking at the rainfall process and its generation throughout the United States at the annual and seasonal scales. The analysis also catalogs a wide range of regional and seasonal rainfall-atmospheric variables dependencies, which provide the basis for future comparison and improved understanding of how both natural and anthropogenic climate variability will affect the properties of the regional rainfall process.

Acknowledgments. CL was partially supported by the National Science Foundation (AGS1243204), the

Lamont-Doherty Earth Observatory, and Columbia's Department of Earth and Environmental Sciences. CL, JTA, and MKT acknowledge funding from the Office of Naval Research (N00014-12-1-0911). We are grateful to Tanvir Ahmed and Seonkyoo Yoon for the processing and quality control of the rainfall gauge data.

REFERENCES

Allen, J. T., and D. J. Karoly, 2014: A climatology of Australian severe thunderstorm environments 1979–2011: Inter-annual variability and ENSO influence. *Int. J. Climatol.*, **34**, 81–97, doi:10.1002/joc.3667.

——, ——, and G. A. Mills, 2011: A severe thunderstorm climatology for Australia and associated thunderstorm environments. *Aust. Meteor. Oceanogr. J.*, **61**, 143–158.

——, M. K. Tippett, and A. H. Sobel, 2015a: An empirical model relating U.S. monthly hail occurrence to large-scale meteorological environment. *J. Adv. Model. Earth Syst.*, **7**, 226–243, doi:10.1002/2014MS000397.

——, ——, and ——, 2015b: Influence of the El Nino/Southern Oscillation on tornado and hail frequency in the United States. *Nat. Geosci.*, **8**, 278–283, doi:10.1038/ngeo2385.

Baldwin, M. E., J. S. Kain, and M. P. Kay, 2002: Properties of the convection scheme in NCEP's Eta Model that affect forecast sounding interpretation. *Wea. Forecasting*, **17**, 1063–1079, doi:10.1175/1520-0434(2002)017<1063:POTCSI>2.0.CO;2.

Berg, P., J. Haerter, P. Thejll, C. Piani, S. Hagemann, and J. Christensen, 2009: Seasonal characteristics of the relationship between daily precipitation intensity and surface temperature. *J. Geophys. Res.*, **114**, D18102, doi:10.1029/2009JD012008.

Brooks, H. E., J. W. Lee, and J. P. Craven, 2003: The spatial distribution of severe thunderstorm and tornado environments from global reanalysis data. *Atmos. Res.*, **67–68**, 73–94, doi:10.1016/S0169-8095(03)00045-0.

Bukovsky, M. S., and D. J. Karoly, 2007: A brief evaluation of precipitation from the North American Regional Reanalysis. *J. Hydrometeor.*, **8**, 837–846, doi:10.1175/JHM595.1.

Camargo, S. J., K. A. Emanuel, and A. H. Sobel, 2007: Use of a genesis potential index to diagnose ENSO effects on tropical cyclone genesis. *J. Climate*, **20**, 4819–4834, doi:10.1175/JCLI4282.1.

——, M. Tippett, A. Sobel, G. Vecchi, and M. Zhao, 2014: Testing the performance of tropical cyclone genesis indices in future climates using the HIRAM model. *J. Climate*, **27**, 9171–9196, doi:10.1175/JCLI-D-13-00505.1.

DeGaetano, A. T., 2009: Time-dependent changes in extreme-precipitation return-period amounts in the continental United States. *J. Appl. Meteor. Climatol.*, **48**, 2086–2099, doi:10.1175/2009JAMC2179.1.

Diffenbaugh, N. S., M. Scherer, and R. J. Trapp, 2013: Robust increases in severe thunderstorm environments in response to greenhouse forcing. *Proc. Natl. Acad. Sci. USA*, **110**, 16 361–16 366, doi:10.1073/pnas.1307758110.

Doswell, C. A., III, H. E. Brooks, and R. A. Maddox, 1996: Flash flood forecasting: An ingredients-based methodology. *Wea. Forecasting*, **11**, 560–581, doi:10.1175/1520-0434(1996)011<0560:FFFAIB>2.0.CO;2.

Gensini, V. A., T. L. Mote, and H. E. Brooks, 2014: Severe-thunderstorm reanalysis environments and collocated radiosonde observations. *J. Appl. Meteor. Climatol.*, **53**, 742–751, doi:10.1175/JAMC-D-13-0263.1.

Groisman, P. Ya., R. W. Knight, D. R. Easterling, T. R. Karl, G. C. Hegerl, and V. N. Razuvaev, 2005: Trends in intense precipitation in the climate record. *J. Climate*, **18**, 1326–1350, doi:10.1175/JCLI3339.1.

——, ——, and T. R. Karl, 2012: Changes in intense precipitation over the central United States. *J. Hydrometeor.*, **13**, 47–66, doi:10.1175/JHM-D-11-039.1.

Haerter, J. O., and P. Berg, 2009: Unexpected rise in extreme precipitation caused by a shift in rain type? *Nat. Geosci.*, **2**, 372–373, doi:10.1038/ngeo523.

Hertig, E., and J. Jacobeit, 2013: A novel approach to statistical downscaling considering nonstationarities: Application to daily precipitation in the Mediterranean area. *J. Geophys. Res. Atmos.*, **118**, 520–533, doi:10.1002/jgrd.50112.

Hitchens, N. M., H. E. Brooks, and R. S. Schumacher, 2013: Spatial and temporal characteristics of heavy hourly rainfall in the United States. *Mon. Wea. Rev.*, **141**, 4564–4575, doi:10.1175/MWR-D-12-00297.1.

Lenderink, G., and E. Van Meijgaard, 2008: Increase in hourly precipitation extremes beyond expectations from temperature changes. *Nat. Geosci.*, **1**, 511–514, doi:10.1038/ngeo262.

——, and ——, 2009: Unexpected rise in extreme precipitation caused by a shift in rain type? *Nat. Geosci.*, **2**, 373–373, doi:10.1038/ngeo524.

Lepore, C., D. Veneziano, and A. Molini, 2015: Temperature and CAPE dependence of rainfall extremes in the eastern United States. *Geophys. Res. Lett.*, **42**, 74–83, doi:10.1002/2014GL062247.

Li, H., and B. A. Colle, 2014: Multidecadal changes in the frequency and ambient conditions of warm season convective storms over the northeastern United States. *J. Climate*, **27**, 7285–7300, doi:10.1175/JCLI-D-13-00785.1.

Marsh, P. T., H. E. Brooks, and D. J. Karoly, 2007: Assessment of the severe weather environment in North America simulated by a global climate model. *Atmos. Sci. Lett.*, **8**, 100–106, doi:10.1002/asl.159.

Mesinger, F., and Coauthors, 2006: North American Regional Reanalysis. *Bull. Amer. Meteor. Soc.*, **87**, 343–360, doi:10.1175/BAMS-87-3-343.

Molini, L., A. Parodi, N. Rebora, and G. C. Craig, 2011: Classifying severe rainfall events over Italy by hydrometeorological and dynamical criteria. *Quart. J. Roy. Meteor. Soc.*, **137**, 148–154, doi:10.1002/qj.741.

Myoung, B., and J. W. Nielsen-Gammon, 2010: Sensitivity of monthly convective precipitation to environmental conditions. *J. Climate*, **23**, 166–188, doi:10.1175/2009JCLI2792.1.

Ralph, F. M., and Coauthors, 2005: Improving short-term (0–48 h) cool-season quantitative precipitation forecasting: Recommendations from a USWRP workshop. *Bull. Amer. Meteor. Soc.*, **86**, 1619–1632, doi:10.1175/BAMS-86-11-1619.

——, P. J. Neiman, G. A. Wick, S. I. Gutman, M. D. Dettinger, D. R. Cayan, and A. B. White, 2006: Flooding on California's Russian River: Role of atmospheric rivers. *Geophys. Res. Lett.*, **33**, L13801, doi:10.1029/2006GL026689.

Rudolph, J. V., and K. Friedrich, 2014: Dynamic and thermodynamic predictors of vertical structure in radar-observed regional precipitation. *J. Climate*, **27**, 2143–2158, doi:10.1175/JCLI-D-13-00239.1.

Shaw, S. B., A. A. Royem, and S. J. Riha, 2011: The relationship between extreme hourly precipitation and surface temperature in different hydroclimatic regions of the United States. *J. Hydrometeor.*, **12**, 319–325, doi:10.1175/2011JHM1364.1.

Singh, M. S., and P. A. O'Gorman, 2014: Influence of microphysics on the scaling of precipitation extremes with temperature. *Geophys. Res. Lett.*, **41**, 6037–6044, doi:10.1002/2014GL061222.

Smith, B. L., S. E. Yuter, P. J. Neiman, and D. Kingsmill, 2010: Water vapor fluxes and orographic precipitation over northern California associated with a landfalling atmospheric river. *Mon. Wea. Rev.*, **138**, 74–100, doi:10.1175/2009MWR2939.1.

Steinschneider, S., and U. Lall, 2015: A hierarchical Bayesian regional model for nonstationary precipitation extremes in northern California conditioned on tropical moisture exports. *Water Resour. Res.*, **51**, 1472–1492, doi:10.1002/2014WR016664.

Tippett, M. K., S. J. Camargo, and A. H. Sobel, 2011: A Poisson regression index for tropical cyclone genesis and the role of large-scale vorticity in genesis. *J. Climate*, **24**, 2335–2357, doi:10.1175/2010JCLI3811.1.

——, A. H. Sobel, and S. J. Camargo, 2012: Association of U.S. tornado occurrence with monthly environmental parameters. *Geophys. Res. Lett.*, **39**, L02801, doi:10.1029/2011GL050368.

——, ——, ——, and J. T. Allen, 2014: An empirical relation between U.S. tornado activity and monthly environmental parameters. *J. Climate*, **27**, 2983–2999, doi:10.1175/JCLI-D-13-00345.1.

Trapp, R. J., N. S. Diffenbaugh, H. E. Brooks, M. E. Baldwin, E. D. Robinson, and J. S. Pal, 2007: Changes in severe thunderstorm environment frequency during the 21st century caused by anthropogenically enhanced global radiative forcing. *Proc. Natl. Acad. Sci. USA*, **104**, 19 719–19 723, doi:10.1073/pnas.0705494104.

Utsumi, N., S. Seto, S. Kanae, E. E. Maeda, and T. Oki, 2011: Does higher surface temperature intensify extreme precipitation? *Geophys. Res. Lett.*, **38**, L16708, doi:10.1029/2011GL048426.

Vecchi, G. A., M. Zhao, H. Wang, G. Villarini, A. Rosati, A. Kumar, I. M. Held, and R. Gudgel, 2011: Statistical–dynamical predictions of seasonal North Atlantic hurricane activity. *Mon. Wea. Rev.*, **139**, 1070–1082, doi:10.1175/2010MWR3499.1.

West, G. L., W. J. Steenburgh, and W. Y. Cheng, 2007: Spurious grid-scale precipitation in the North American Regional Reanalysis. *Mon. Wea. Rev.*, **135**, 2168–2184, doi:10.1175/MWR3375.1.